



## Control and Analysis of MPPT Techniques for Standalone PV System with High Voltage Gain Interleaved Boost Converter

Jyotheeswara REDDY<sup>1</sup>, Sudhakar NATARAJAN<sup>2,\*</sup>

<sup>1,2</sup>School of Electrical Engineering, Vellore Institute of Technology, Vellore, India.

### Article Info

Received: 10/09/2017

Accepted: 23/12/2017

### Keywords

Photovoltaic (PV)  
Maximum Power Point  
Tracking (MPPT)  
P&O algorithm  
Fuzzy Logic Controller  
(FLC)  
RBFN  
High voltage gain IBC

### Abstract

In photovoltaic (PV) power generating systems DC-DC converters acts as an interface between the PV source and the load. This paper deals with the use of a high voltage gain three-phase interleaved DC-DC boost converter (IBC) for the standalone PV system applications. Interleaving technique provides high power capability and reduces the voltage stress on the power semiconductor devices. In PV system maximum power point tracking (MPPT) technique is used to track the maximum power from the PV panel. To extract the maximum power from the PV panel at different irradiation levels radial basis function network (RBFN) based MPPT algorithm is developed. The output power of the high voltage gain three-phase IBC with RBFN based MPPT controller is compared with traditional P&O and fuzzy logic based MPPT controllers at different irradiation levels. The performance analysis of P&O, fuzzy logic and RBFN MPPT algorithms with high voltage gain three-phase IBC is done by using MATLAB/SIMULINK.

### Nomenclature:

$V_{pv}$ : PV panel output voltage (V)

$I_{pv}$ : PV panel output current (A)

$I$ : PV Cell phase current (A)

$I_D$ : Diode saturation current of PV panel (A)

$q$ : Electron charge ( $1.698 \times 10^{-19}$  C)

$k$ : Boltzman constant ( $1.38 \times 10^{-23}$  J/K)

$N_s$ : Number of cells connected in series

$R_s$ : Series resistances of the cell

$R_{sh}$ : Parallel resistances of the cell

$T$ : Absolute temperature

$V_{oc}$ : Open circuit voltage of PV panel (V)

$I_{sc}$ : Short circuit Current PV panel (A)

$V_o$ : output voltage

$G$ : Solar irradiation of PV panel

$K$ : Duty cycle

$M$ : voltage gain of converter

$f_s$ : Switching frequency of the converter

$I_o$ : output current

## 1. INTRODUCTION

Due to the exhaustion of oil resources and fossil fuels, renewable energy resources gained a very high demand. In recent years, among the entire available renewable sources solar energy is becoming more popular due to its low maintenance, pollution-free operation and absence of fuel cost [1,2]. But the major drawback of the solar PV system is the overall energy conversion efficiency of the PV array is very low. The maximum power point (MPP) of the system changes with irradiation level and temperature due to non-linear characteristics of the PV module. In order to achieve maximum efficiency, it is necessary to use MPPT algorithms to track the maximum available power from the PV module at different irradiation levels.

There are different MPPT techniques available like perturb and observe (P&O), parctical swarm optimization (PSO), incremental conductance (INC), fuzzy logic controller (FLC), neural network (NN),

\*Corresponding author, e-mail: nsudhakar@vit.ac.in

adaptive neuro-fuzzy inference system (ANFIS), genetic algorithm, artificial BEE Colony to track MPP [3,4]. Among all the available MPPT algorithms, P&O is simple, popular and easy to implement. This algorithm is based on observation of PV module output power and its perturbation by changing the current or voltage of the PV module. Incremental conductance method is based on the slope of power vs. current (voltage) curve. At the maximum power point the slope of power vs. current (voltage) curve is zero. Incremental conductance algorithm will give fast and accurate tracking of MPP. P&O and incremental conductance methods will produce oscillations at steady state which will reduce the efficiency of the PV system [5]. To overcome this problem fuzzy logic controller and neural network algorithms are introduced to track the MPP with increased efficiency and accuracy. In this paper, radial basis function network (RBFN) which is one of the neural network methods is used to track the MPP. RBFN effectively controls the time varying and non-linear conditions [6,7].

The output voltage of PV module is very low. So, DC-DC boost converter is used to boost the PV module output voltage. Boost converter, buck-boost converter, Cuk converter, SEPIC converter, flyback converter, interleaved boost converter and push-pull converter are widely used different DC-DC converter topologies for PV systems [8,9]. In this paper, a high voltage gain three-phase IBC is designed to reduce the input current ripples. Interleaving technique increases the reliability of PV module and provides high power capability. The block diagram MPPT controlled PV system is as shown in the Fig. 1. The sensed voltage and current outputs from the PV panel are given as inputs to the MPPT controller to track the MPP and it generates a duty cycle to the DC-DC converter.

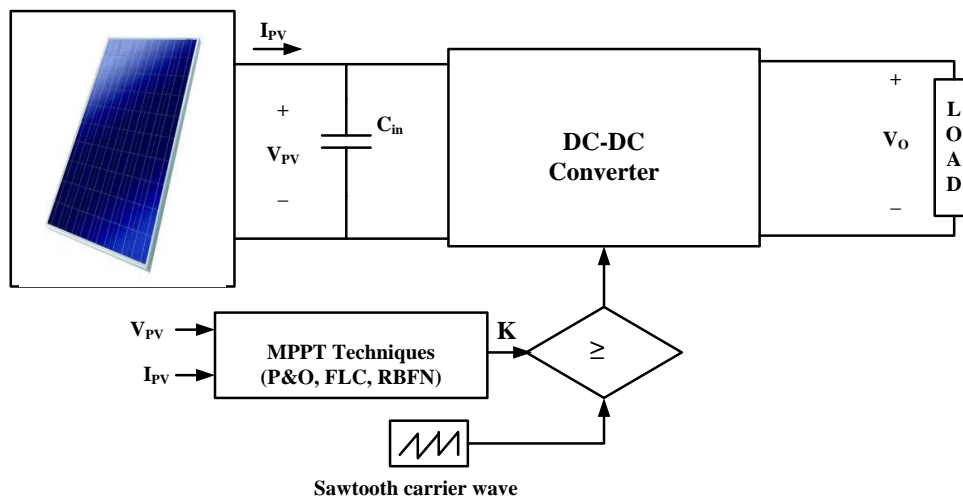


**Figure 1.** PV system with MPPT controller

This paper is ordered as follows. In section 2, modeling of PV module is discussed. Section 3 discusses the analysis of high voltage gain three-phase IBC. Section 4 discusses techniques and finally the simulation results are discussed in section 5.

## 2. MODELING OF PV ARRAY

PV cell is an electrical device, which converts radiation of solar energy into electrical energy directly. The PV cells are made up of with semiconductor materials like silicon. Different models are available for PV cells such as single diode model, double diode model, first empirical model and second empirical model. Among all these different models single-diode model is simple and commonly used PV cell. The PV cells are connected in parallel or series to obtain the high output current or voltage respectively. The equivalent circuit of the single-diode model of PV cell is as shown in Fig.2 [10]. The circuit consists of current source ( $I_L$ ) in parallel with a diode, series and shunt resistances.

The mathematical modeling of PV cell is done by using the V-I relationship of the PV system.

$$I = I_L - I_D \left[ \exp \left( \frac{q(V + R_S I)}{N_S k T a} \right) - 1 \right] - \frac{V + R_S I}{R_{Sh}} \quad (1)$$

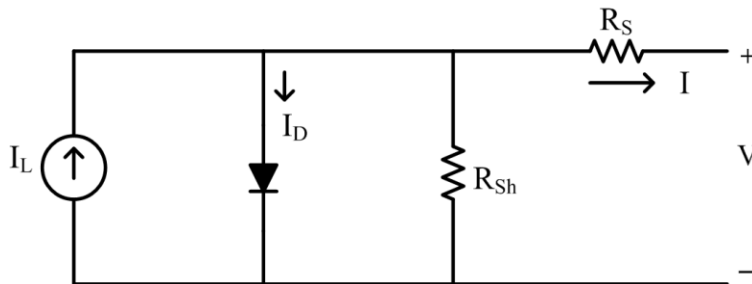
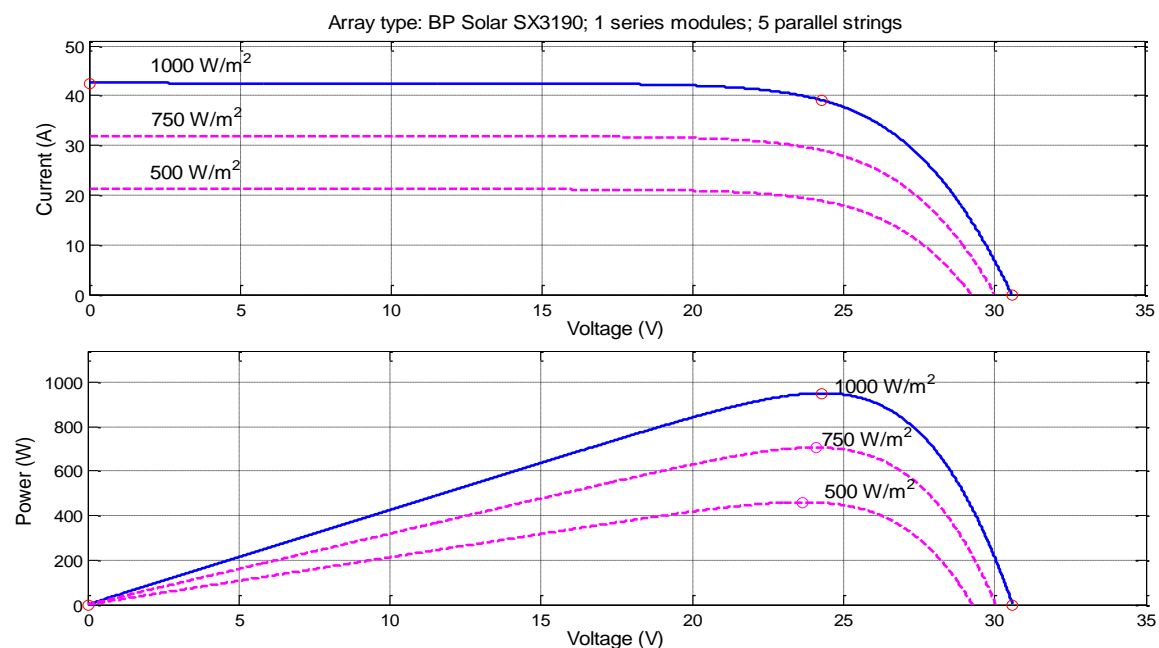


**Figure 2.** PV cell equivalent circuit

**Table 1.** Solar PV module parameters

Description	Rating
Maximum Power ( $P_{max}$ )	950 W
Maximum Voltage ( $V_{max}$ )	24.3 V
Maximum Current ( $I_{max}$ )	7.829 A
Open circuit Voltage ( $V_{OC}$ )	30.6 V
Short circuit Current ( $I_{SC}$ )	8.51 A
Irradiation (G)	800-1000 W/m <sup>2</sup>
Temperature (T)	25 <sup>o</sup> C
No. of PV cells connected in parallel	5

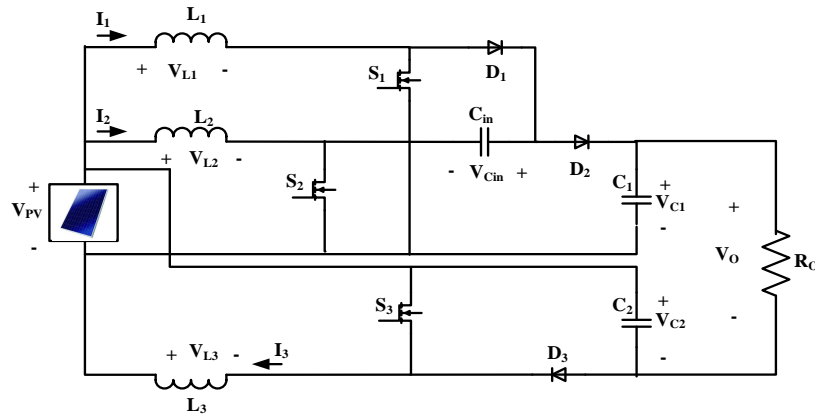
The V-I and P-V characteristics of PV module at a constant temperature of 25°C and at different irradiation levels of 1000 W/m<sup>2</sup>, 750 W/m<sup>2</sup> and 500 W/m<sup>2</sup> are shown in Fig. 3. The output power of the solar cell depends on the irradiation value. If the irradiation is high then PV module will give maximum power otherwise vice versa [11]. A DC-DC converter is connected to the output of the PV module to maintain a constant voltage across the DC link.



**Figure 3.** PV cell characteristics at different irradiation conditions

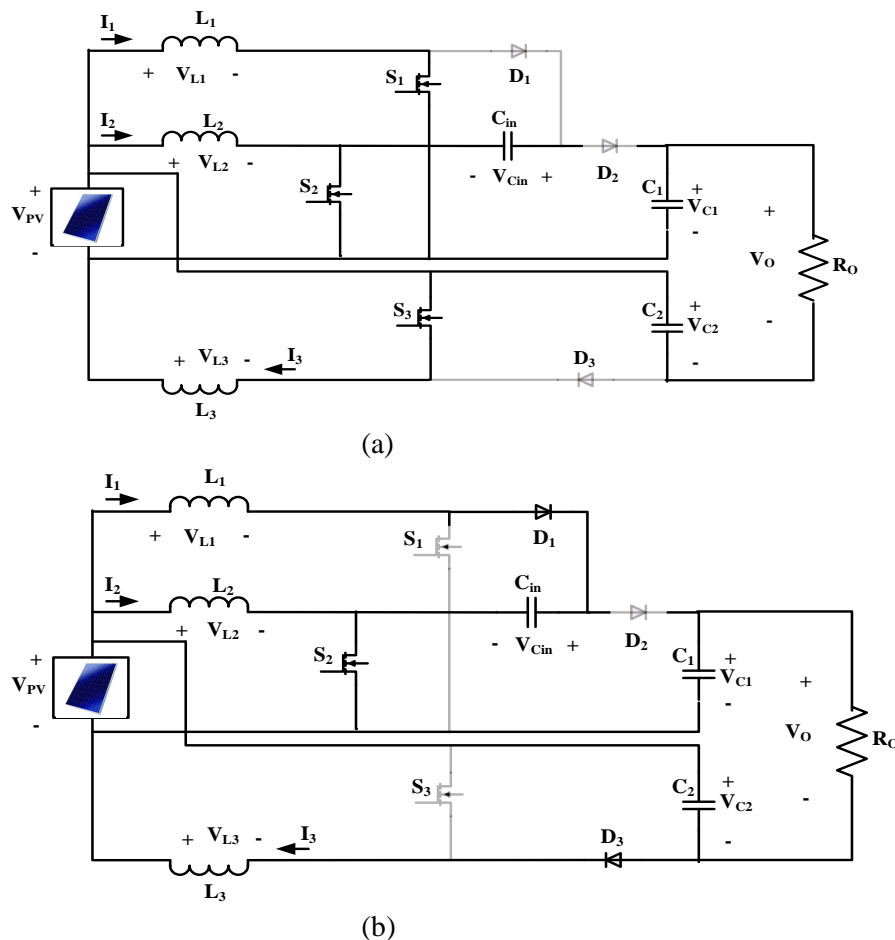
### 3. HIGH VOLTAGE GAIN THREE-PHASE IBC

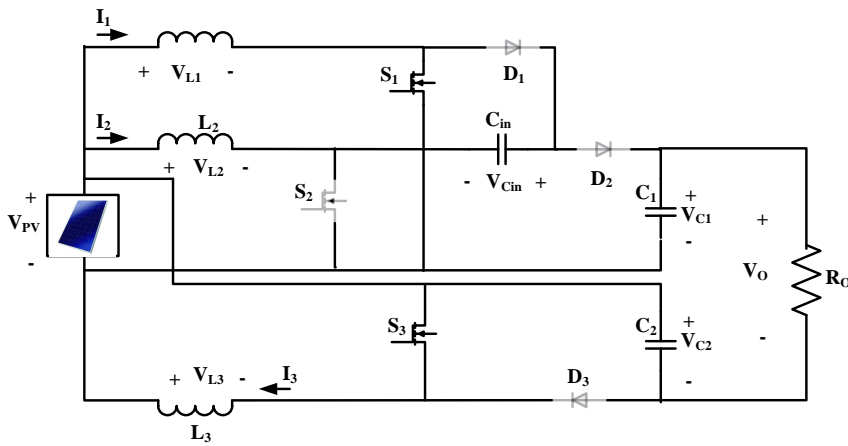
The circuit topology of high voltage gain three-phase IBC is as shown in Fig. 4. The circuit consists of three switches ( $S_1$ ,  $S_2$  &  $S_3$ ) and three diodes ( $D_1$ ,  $D_2$  &  $D_3$ ).  $L_1$ ,  $L_2$  and  $L_3$  are the filtering inductors of phase-1, phase-2 and phase-3 respectively.  $V_{PV}$  is the input voltage,  $V_O$  is output voltage and  $R_O$  is the load resistor.



**Figure 4.** Circuit diagram of high voltage gain three-phase IBC

The switches  $S_1$ ,  $S_2$  and  $S_3$  are switched ON by using two gate pulses which are  $180^\circ$  phase shifted. One gate pulse is given to the switch  $S_2$  and another gate pulse with  $180^\circ$  phase shift is given to the switches  $S_1$  and  $S_3$  [12]. The operating modes of the converter are as shown in Fig. 5 and the steady-state characteristics are as shown in the Fig. 6.





(c)

Figure 5. Modes of operation of high voltage gain three-phase IBC

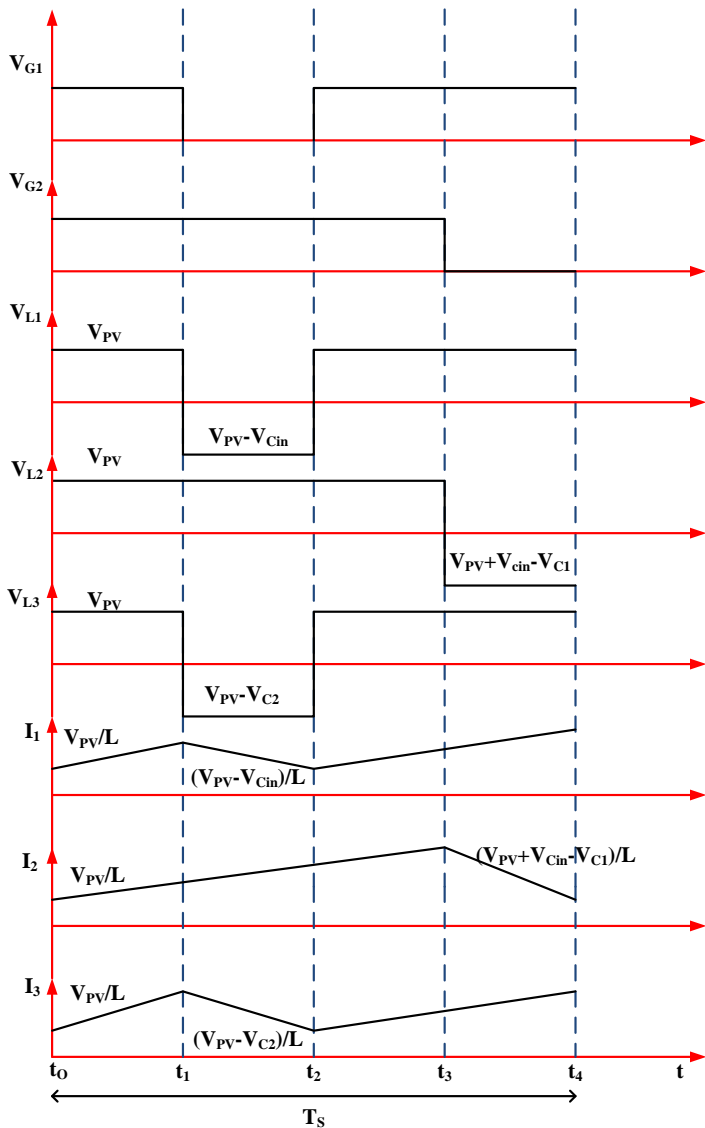


Figure 6. Steady-state waveforms of high voltage gain three-Phase IBC

**Mode-1 ( $t_0 \leq t \leq t_1$ ):** During this mode, all the three switches  $S_1, S_2$  &  $S_3$  are conducting and all the three diodes  $D_1, D_2$  &  $D_3$  are in reverse biased as shown in Fig. 5(a). The input voltage source  $V_{PV}$  charges the inductors  $L_1, L_2$  &  $L_3$ . The current through these inductors  $I_1, I_2$  &  $I_3$  increases linearly with a slope of

$V_{PV}/L$ . The input capacitor  $C_{in}$  is disconnected from the load as well as from the supply. The output capacitors  $C_1$  &  $C_2$  supplies the energy to the load resistor and the output capacitor voltages  $V_{C1}$  and  $V_{C2}$  decreases with a slope of  $-V_O/R_0C$ .

**Mode-2 ( $t_1 \leq t \leq t_2$ ):** In this mode, the switch  $S_2$  is conducting and the switches  $S_1$  and  $S_3$  are switched OFF. The diodes  $D_1$  and  $D_3$  are forward biased and the diode  $D_2$  is reverse biased as shown in Fig. 5(b). The currents through the inductors  $L_1$  and  $L_3$  are decreases with slopes of  $(V_{PV} - V_{Cin})/L$  and  $(V_{PV} - V_{C2})/L$  respectively. The current through the inductor  $L_2$  increases with a slope of  $V_{FC}/L$ . The capacitor  $C_1$  supplies the energy to the load and the capacitors  $C_2$  and  $C_{in}$  are gets charged by the input voltage  $V_{PV}$ .

**Mode-3 ( $t_3 \leq t \leq t_4$ ):** This mode is similar to mode-1. All the three switches  $S_1$ ,  $S_2$  &  $S_3$  are conducting and all the three diodes  $D_1$ ,  $D_2$  &  $D_3$  are in reverse bias condition.

**Mode-4 ( $t_4 \leq t \leq t_5$ ):** In this mode, the switch  $S_2$  is switched OFF and the switches  $S_1$  and  $S_3$  are switched ON. The diodes  $D_1$  and  $D_3$  are reverse biased and the diode  $D_2$  is conducting as shown in Fig. 5(c). The input voltage source  $V_{PV}$  charges the inductors  $L_1$  and  $L_3$  and the current through these inductors increases with a slope of  $V_{PV}/L$ . The current through the inductor  $L_2$  decreases with a slope of  $(V_{PV} + V_{Cin} - V_{C1})/L$ . The capacitors  $C_2$  and  $C_{in}$  supplies the energy to the load and the capacitor  $C_1$  gets charged by the input voltage  $V_{PV}$ .

### 3.1. Analysis of the Converter

To simplify the analysis of the converter, inductors, capacitors and power semiconductor devices are assumed to be ideal and the converter operating in CCM.

The static voltage gain (M) of the DC-DC converter is obtained by applying volt-second balance on inductors  $L_1$ ,  $L_2$  and  $L_3$ . Now by applying volt-second balance to the inductor  $L_1$ , we get

$$V_{L1} = V_{PV}(t_1 - t_0) + (V_{PV} - V_{Cin})(t_2 - t_1) + V_{PV}(t_3 - t_2) + V_{PV}(t_4 - t_3) = 0 \quad (2)$$

From Eq. (2) the input capacitor voltage  $V_{Cin}$  is given as

$$V_{Cin} = \frac{V_{PV}}{(1 - K)} \quad (3)$$

Where K is duty cycle. Now by applying volt-second balance to the inductor  $L_2$ , we get

$$V_{L2} = V_{PV}(t_1 - t_0) + V_{PV}(t_2 - t_1) + V_{PV}(t_3 - t_2) + (V_{PV} + V_{Cin} - V_{C1})(t_4 - t_3) = 0 \quad (4)$$

Solving Eq. (4) yields

$$V_{C1} = \frac{V_{PV}}{(1 - K)} + V_{Cin} \quad (5)$$

From Eq. (3) and Eq. (5) we get

$$V_{C1} = \frac{2V_{PV}}{(1 - K)} \quad (6)$$

By applying volt-second balance to the inductor  $L_3$ , we get

$$V_{L3} = V_{PV}(t_1 - t_0) + (V_{PV} - V_{C2})(t_2 - t_1) + V_{PV}(t_3 - t_2) + V_{PV}(t_4 - t_3) = 0 \quad (7)$$

From Eq. (7), capacitor  $C_2$  voltage is obtained as

$$V_{C2} = \frac{V_{PV}}{(1-K)} \quad (8)$$

The output voltage of the converter is given as

$$V_O = V_{C1} + V_{C2} - V_{PV} \quad (9)$$

By substituting, Eqs. (6) and (8) in (9), the converter static voltage gain M is obtained as

$$M = \frac{V_O}{V_{PV}} = \frac{(2+K)}{(1-K)} \quad (10)$$

The voltage gain of the converter with respect to duty cycle (K) is as shown in Fig. 7.

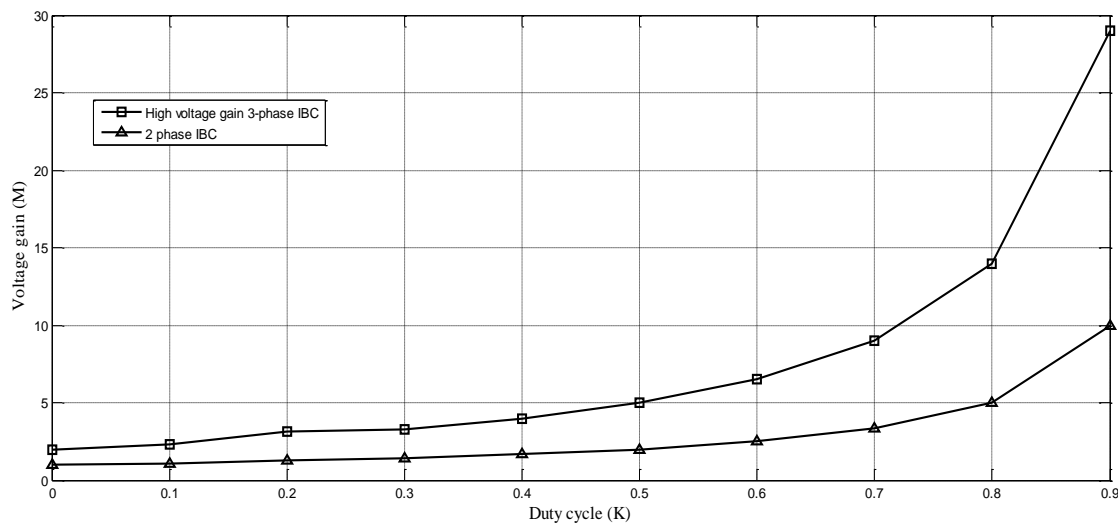


**Figure 7.** Voltage gain comparison of high voltage gain IBC with 2-phase IBC

The switches  $S_1$  and  $S_3$  are switched OFF in mode-2 and remains switched ON in all the other modes. From Fig. 5(b), the voltage stress of switches  $S_1$  and  $S_2$  can be expressed as

$$V_{S1} = V_{Cin} = \frac{V_{PV}}{(1-K)} \quad (11)$$

$$V_{S2} = V_{C1} - V_{Cin} = \frac{V_{PV}}{(1-K)} \quad (12)$$

The switch  $S_2$  is switched OFF in only mode-4. From Fig. 5(c), the voltage stress of switch  $S_3$  is expressed as

$$V_{S3} = V_{C2} = \frac{V_{PV}}{(1-K)} \quad (13)$$

In the same way the voltage stress of the diodes  $D_1$ ,  $D_2$  and  $D_3$  can be derived and they expressed as

$$V_{D1} = -V_{C1} = -\frac{2V_{PV}}{(1-K)} \quad (14)$$

$$V_{D2} = V_{Cin} - V_{C2} = -\frac{V_{PV}}{(1-K)} \quad (15)$$

$$V_{D3} = V_{C2} = \frac{V_{PV}}{(1-K)} \quad (16)$$

The inductance L is designed by using the input current ripple ( $\Delta I$ ). The maximum input current ripple is assumed as 20% of the input current, the value of the input inductor is calculated by using the Eq. (17).

$$L = L_1 = L_2 = L_3 = \frac{KV_{PV}}{\Delta I f_S} \quad (17)$$

Similarly, the input and output capacitor is designed by using the voltage ripple across the input and output capacitors. The voltage ripple ( $\Delta V$ ) is considered as 10% of the output voltage.

$$C_{in} = \frac{V_O}{R_O \Delta V_{C_{in}} f_S} \quad (18)$$

$$C = C_1 = C_2 = \frac{KV_O}{R_O \Delta V f_S} \quad (19)$$

The high voltage gain three-phase IBC specifications are listed in Table 2.

**Table 2. Converter Parameters**

Parameter	Value
Switching frequency ( $f_S$ )	50 kHz
Inductor ( $L=L_1=L_2=L_3$ )	1.64 mH
Capacitor ( $C=C_1=C_2$ )	317 $\mu$ F
Input capacitor ( $C_{in}$ )	470 $\mu$ F
Load resistor ( $R_O$ )	42 $\Omega$

#### 4. MPPT CONTROLLER

MPPT is needful for PV system to extract the maximum power from it at different temperature conditions. Among all the available MPPT techniques P&O and INC methods are more popular due to their simple structure and easy operation. These methods may produce oscillations at steady state which will reduce the efficiency of the PV system. To overcome this problem fuzzy logic controller and neural network algorithms are introduced to track the MPP with increased efficiency and accuracy. In this paper neural network based RBFN MPPT controller is developed for standalone PV system and the results of this are compared with conventional P&O and FLC based MPPT techniques.

##### 4.1. P&O based MPPT

P&O MPPT controller is one of the popular and simple technique to track the maximum power from the solar PV system. P&O algorithm is operated by decreasing or increasing the PV array terminal voltage or current periodically and then the PV module output power  $P(k)$  is compared with the previous sample power  $P(k-1)$ . If  $P(k)$  is increased then the PV terminal voltage will be moved in positive direction, otherwise vice versa [13].

The flowchart of P&O MPPT controller is as shown in Fig. 8. If the perturbation step size is low then the oscillations around maximum power point will be less and if it is high then oscillations will also high at MPP. The main disadvantage of the P&O controller is it produces oscillations at steady state which will reduce the efficiency of the PV system.

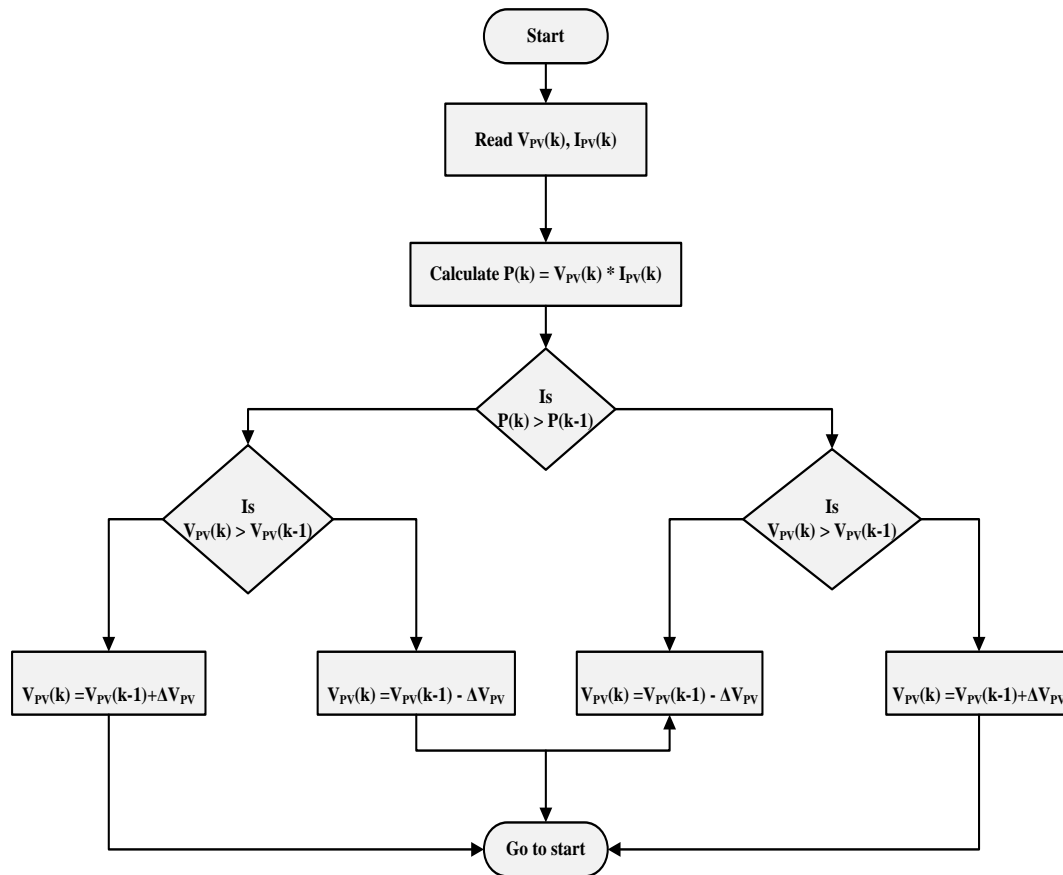


Figure 8. Flowchart for P&O MPPT algorithm

4.2. Fuzzy logic controller (FLC) based MPPT

MPPT by using FLC has the benefits of simple design and better performance. FLC does not require the knowledge of the exact system model. FLC consists of fuzzification, rule base, inference engine and defuzzification as shown in Fig. 9. Appropriate design of fuzzy rules gives the optimal performance of the system [14,15].

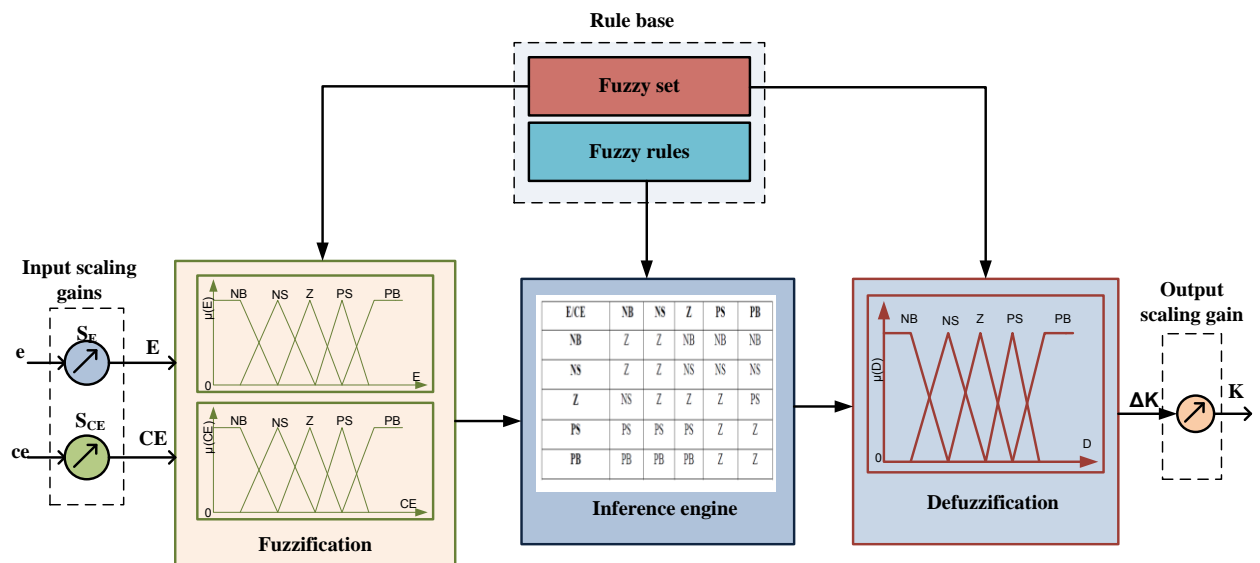


Figure 9. Structure of FLC

The output current and voltage of the PV array are given to the FLC. The input variables to the FLC are error (E) and change in error ( $\Delta E$ ) and the output variable of the FLC is change in duty cycle ( $\Delta K$ ). The error E is set as the change in current with respect to the change in voltage and is given as:

$$E = \frac{I_{PV}(n) - I_{PV}(n-1)}{V_{PV} - V_{PV}(n-1)} \tag{20}$$

The change in error (CE) can be given as

$$CE = E(n) - E(n-1) \tag{21}$$

The rule base of the FLC is designed as illustrated in Table 3 for tracking the MPP with fewer oscillations.

**Table 3.** Fuzzy rule base table

E/CE	NB	NS	Z	PS	PB
NB	Z	Z	NB	NB	NB
NS	Z	Z	NS	NS	NS
Z	NS	Z	Z	Z	PS
PS	PS	PS	PS	Z	Z
PB	PB	PB	PB	Z	Z

**4.3. RBFN based MPPT**

RBFN is a feed-forward neural network model and has both supervised and unsupervised learning phases. RBFN typically consists of three layers: an input layer, a hidden layer and an output layer as shown in Fig.10. The hidden layer consists of non-linear radial basis activation function whereas the output layer is linear one. In this paper, the inputs to the RBFN controller are voltage and current from the PV module and the output is control signal (K) which is given to the boost converter to control the output voltage. The nodes in the input layer are used to transmit the inputs to the hidden layer [16,17].

The net input and output of input layer represented as

$$x_i^{(1)}(n) = net_i^{(1)} \tag{22}$$

$$y_i^{(1)}(n) = f_i^{(1)}[net_i^{(1)}(n)] = net_i^{(1)}(n), i = 1,2 \tag{23}$$

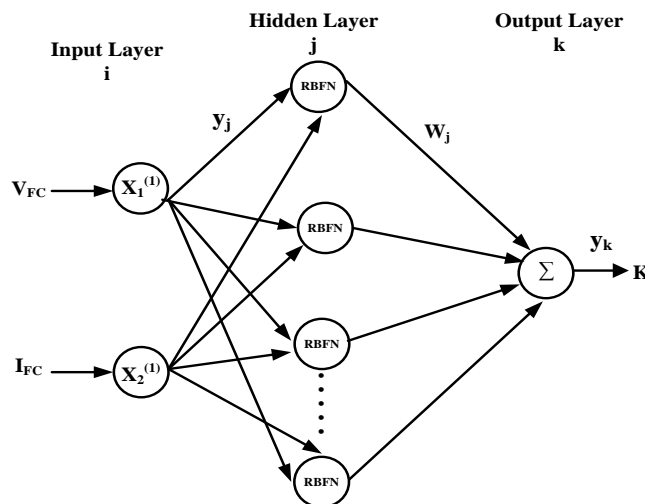


**Figure 10.** RBFN Structure

Where,  $x_i^1$  is input layer,  $y_i^1$  is hidden layer and  $net_i^1$  is the sum of the input layer. Every node in the hidden layer performs a Gaussian function. The Gaussian function is used as a membership function in the RBFN.

$$net_j^{(2)}(n) = -(X - M_j)^T \sum_j (X - M_j) \quad (24)$$

$$y_j^{(2)}(n) = f_j^{(2)} [net_j^{(2)}(n)] \exp[net_j^{(2)}(n)], \quad j = 1, 2, \dots \quad (25)$$

Where,  $M_j$  and  $\sum_j$  are mean and standard deviation of the Gaussian function respectively. The output layer has single node  $t$ , generates the linear control signal ( $K$ ).

$$net_t^{(3)} = \sum_j w_j y_j^{(2)} \quad (26)$$

$$y_t^{(3)} = f_t^{(3)} [net_t^{(3)}(n)] = net_t^{(3)}(n) \quad (27)$$

Where,  $w_j$  is the connective weight matrix between the output and hidden layer. The current and voltage of fuel cell are taken as inputs to the RBFN controller and it produces duty cycle ( $K$ ) as the output as shown in Fig. 11.

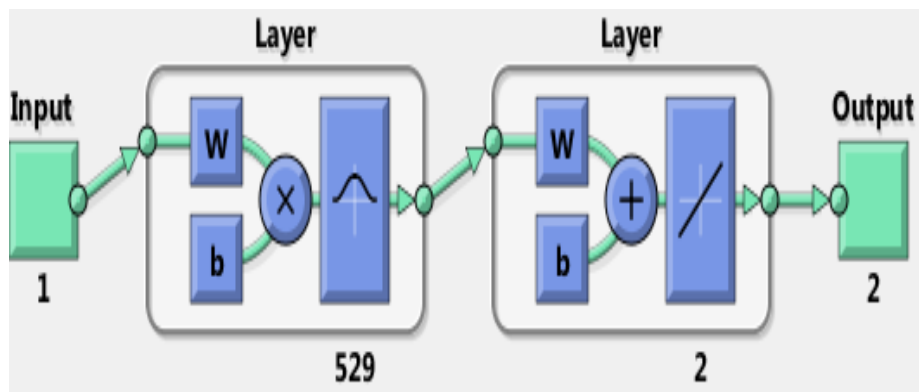


Figure 11. RBFN based MPPT architecture for standalone PV system

## 5. SIMULATION AND RESULTS

The PV module of 950 W is connected to high gain FIBC to form a PV system. By using BP Solar SX 3190 PV module, simulation work is carried out in MATLAB/SIMULINK as shown in Fig. 12. The performance of MPPT using simple P&O, FLC and RBFN algorithms is verified under different irradiation levels. The different irradiation levels are given by using the signal builder block in MATLAB. Different irradiation levels are given as follows: at first from 0 to 0.3s is  $800 \text{ W/m}^2$ , from 0.3 to 0.6s is  $600 \text{ W/m}^2$  and from 0.6 to 0.9s is given as  $1000 \text{ W/m}^2$  as shown in Fig. 13.

For the considered irradianations the output current, voltage and power waveforms of BP Solar SX 3190 PV module are as shown in Fig. 14. It generates a power of 735W for 0 to 0.3 sec, 465W for 0.3sec to 0.6 sec and 940W for 0.6sec to 0.9sec.

The output current, voltage and power of the high voltage gain three-phase IBC by using conventional P&O MPPT controller are as shown in Fig. 15. It generates a power of 608W for 0 to 0.3 sec, 374W for 0.3sec to 0.6 sec and 832W for 0.6sec to 0.9sec at the output of the converter. The output current, voltage and power of the high voltage gain three-phase IBC by using FLC based MPPT controller are as shown in Fig. 16. It generates a power of 640W for 0 to 0.3 sec, 401W for 0.3sec to 0.6 sec and 880W for 0.6sec to 0.9sec at the output of the converter.

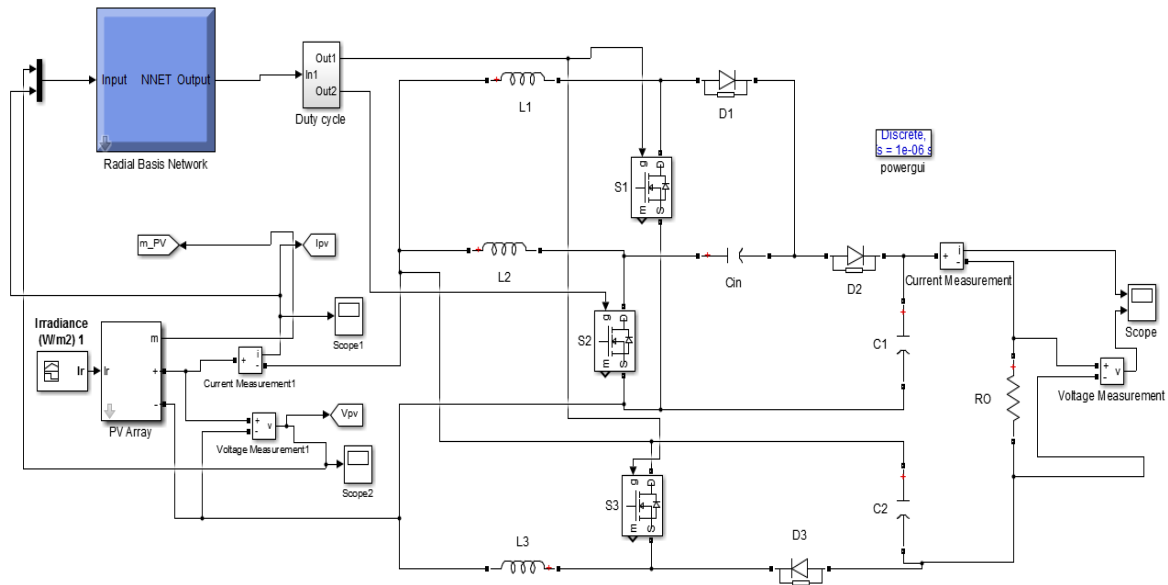


Figure 12. Simulation diagram of Standalone PV system with RBFN MPPT controller

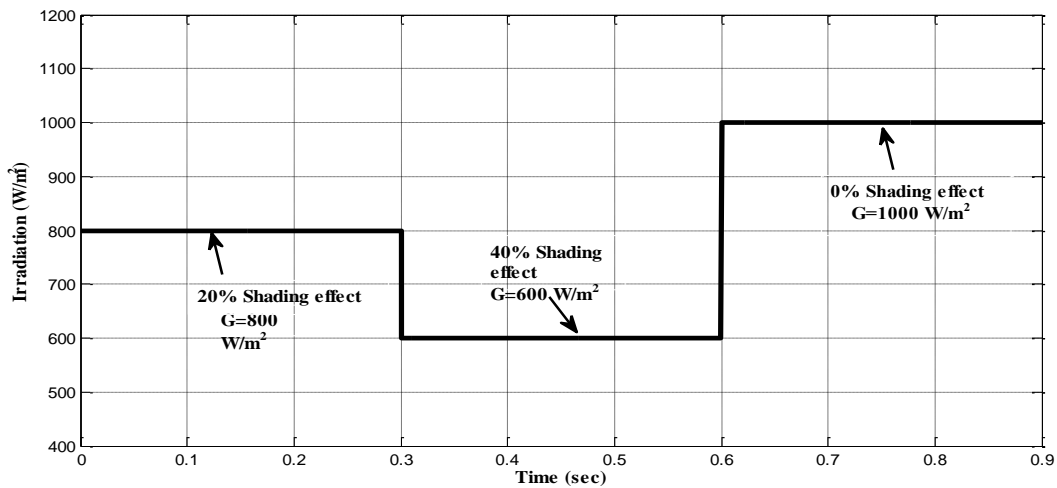


Figure 13. Irradiation change curve

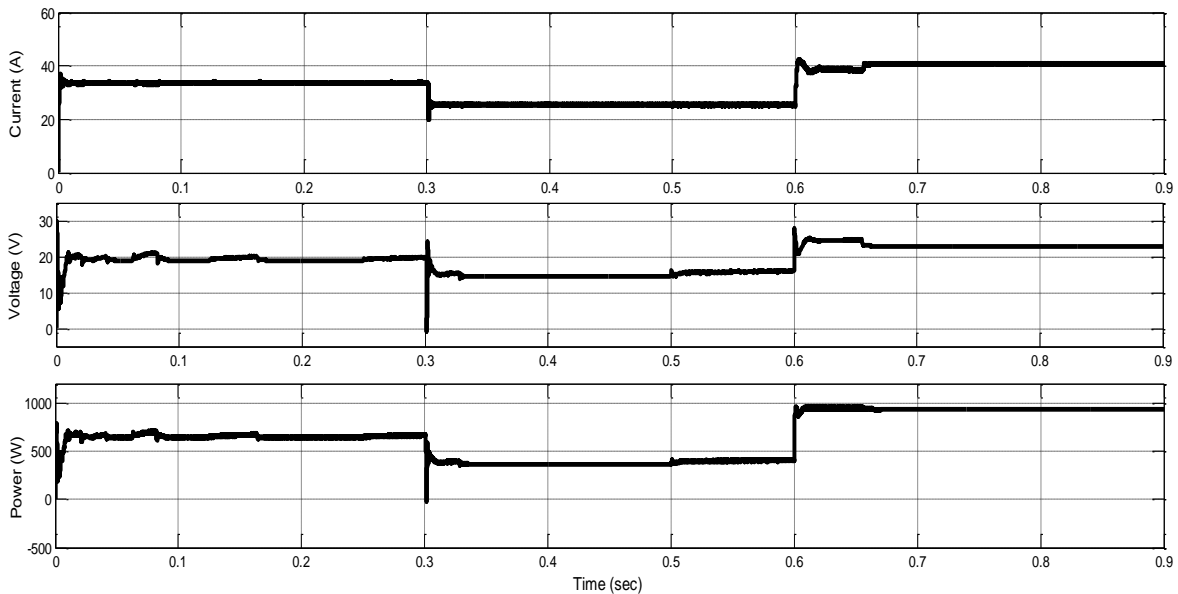


Figure 14. PV panel output current, voltage and power at different irradiancies

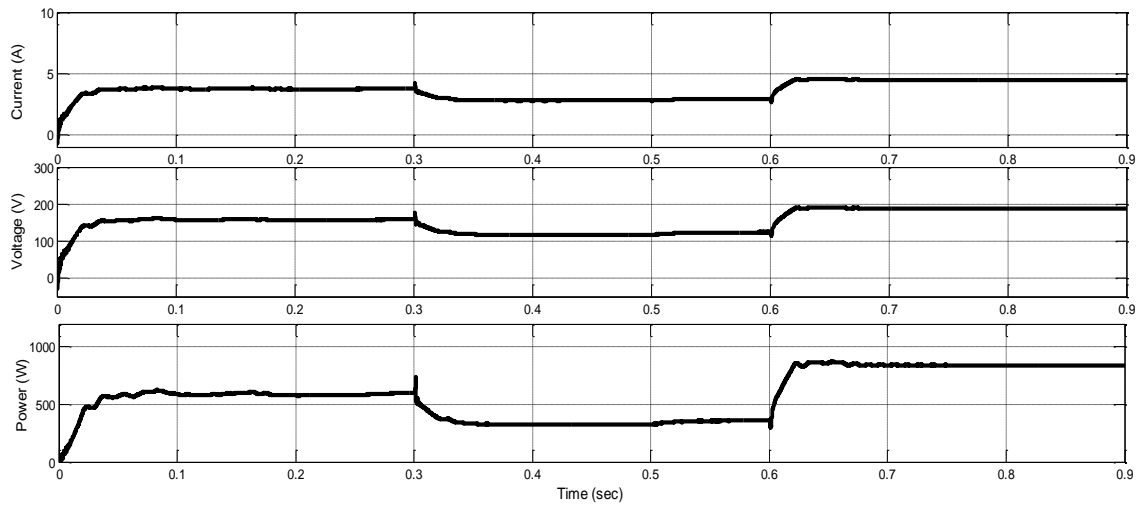


Figure 15. High voltage gain IBC output current, voltage and power with P&O MPPT controller

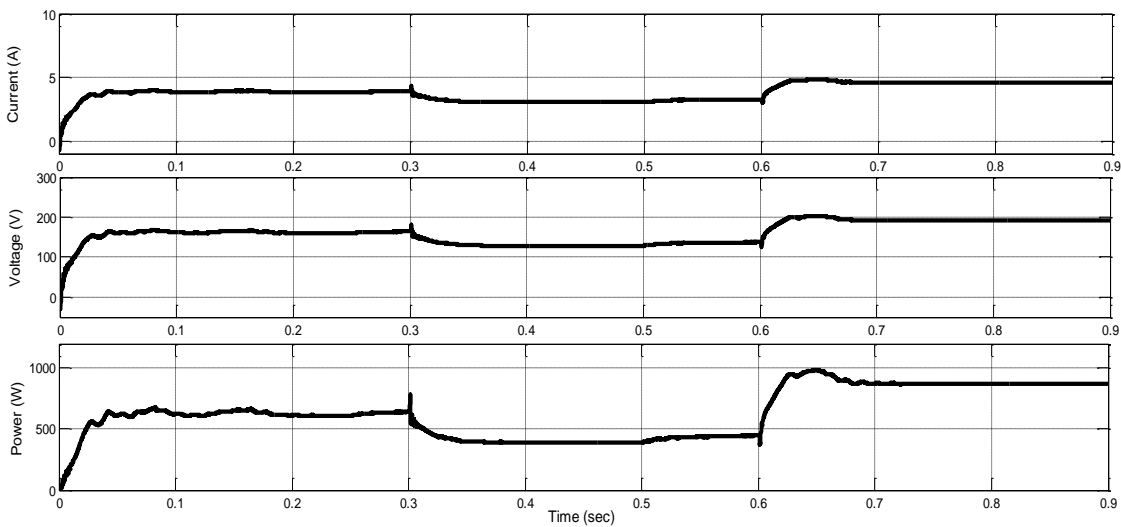


Figure 16. High voltage gain IBC output current, voltage and power with FLC MPPT controller

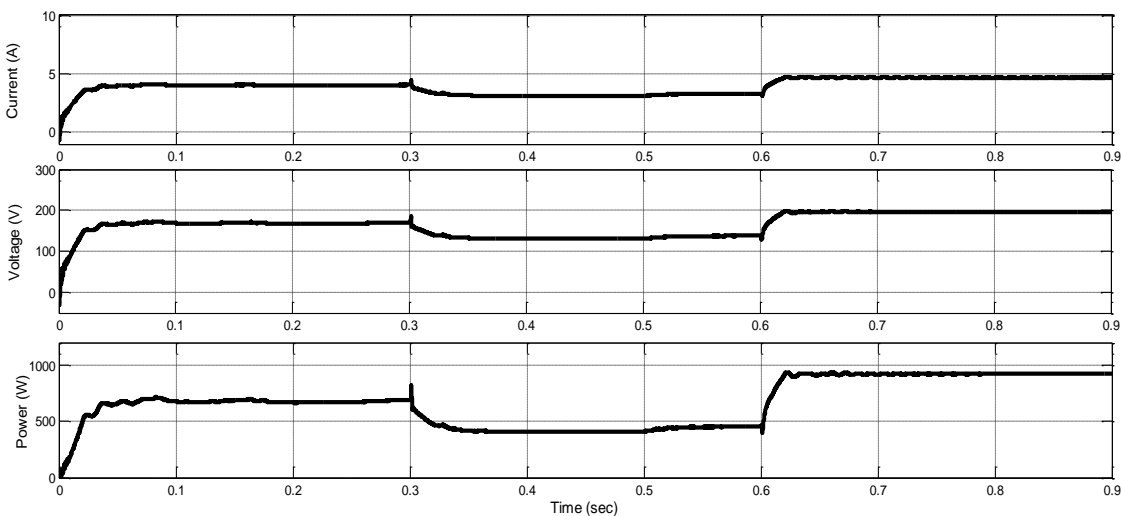
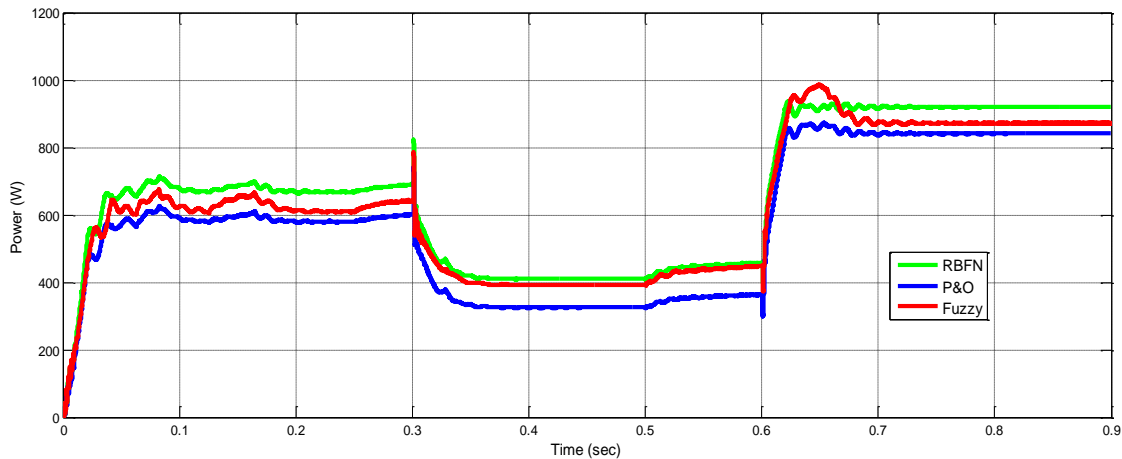


Figure 17. High voltage gain IBC output current, voltage and power with RBFN MPPT controller

The RBFN MPPT controller gives an average load power of 726W for the irradiation of  $800 \text{ W/m}^2$ , 420W for  $600 \text{ W/m}^2$  and 920W for the irradiation of  $1000 \text{ W/m}^2$  as shown in Fig. 17. In Fig. 18, the

performance of the RBFN based MPPT controller of PV module is compared with conventional P&O and FLC based MPPT controllers. From Fig. 18, it is observed that the compared to P&O and FLC the RBFN controller generates the high output power at the DC link. The comparative analyses of these MPPT controllers are listed in Table 4.



**Figure 18.** Comparison of output power with P&O, FLC and RBFN controllers

**Table 4.** Comparison of output power with P&O, FLC and RBFN controllers

Period (Sec)	P&O MPPT			FLC MPPT			RBFN MPPT		
	0-0.3	0.3-0.6	0.6-0.9	0-0.3	0.3-0.6	0.6-0.9	0-0.3	0.3-0.6	0.6-0.9
Solar irradiation (W/m <sup>2</sup> )	800	600	1000	800	600	1000	800	600	1000
Current (A)	4	3.4	4.5	4	3.4	4.68	4.2	3.5	4.84
Voltage (V)	152	110	185	160	118	188	173	120	190
Power (W)	608	374	832	640	401	880	726	420	920

## 6. CONCLUSION

In this paper, a high voltage gain non-isolated three-phase interleaved boost converter is designed for the standalone PV system. The use of 3-phase high voltage gain DC-DC has reduced the PV cell input current ripples and the voltage stress on the semiconductor switches. The RBFN based MPPT technique is developed for 950W BP Solar SX 3190 PV system for extracting the maximum power from it at different irradiation levels. The RBFN based MPPT technique is compared with the conventional P&O and fuzzy logic based MPPT controllers. Simulations results shows that RBFN based MPPT controller can track the maximum power point faster and efficiently, compared to the P&O and fuzzy logic controller.

## CONFLICTS OF INTEREST

No conflict of interest was declared by the authors.

## REFERENCES

- [1] Figueres, E., Garcera, G., Sandia, J., Gonzalez-Espin, F., Rubio, J.C., "Sensitivity study of the dynamics of three-phase photovoltaic inverters with an LCL grid filter", IEEE Transactions on Industrial Electronics, 56(3): 706-717, (2009).

- [2] Li, Q. and Wolfs, P., "A review of the single phase photovoltaic module integrated converter topologies with three different DC link configurations", *IEEE Transactions on Power Electronics*, 23(3): 1320-1333, (2008).
- [3] Ram, J.P., Babu, T.S., Rajasekar, N., "A comprehensive review on solar PV maximum power point tracking techniques", *Renewable and Sustainable Energy Reviews*, 67: 826-847, (2017).
- [4] Saravanan, S., Babu, N.R., "Maximum power point tracking algorithms for photovoltaic system—A review", *Renewable and Sustainable Energy Reviews*, 57: 192-204, (2016).
- [5] Narendiran, S., Sahoo, S.K., Das, R., "Control and Analysis of MPPT Techniques for Maximizing Power Extraction and Eliminating Oscillations in PV System", *International Energy Journal*, 16(3): (2016).
- [6] Seshagiri, S., Khalil, H.K., "Output feedback control of nonlinear systems using RBF neural networks", *IEEE Transactions on Neural Networks*, 11(1): 69-79, (2000).
- [7] Al-Amoudi, A., Zhang, L., "Application of radial basis function networks for solar-array modelling and maximum power-point prediction", *IEE Proceedings-Generation, Transmission and Distribution*, 147(5): 310-316, (2000).
- [8] Li, W., Lv, X., Deng, Y., Liu, J., He, X., "A review of non-isolated high step-up DC/DC converters in renewable energy applications", In *Applied Power Electronics Conference and Exposition, APEC*; 364-369, (2009).
- [9] Kolli, A., Gaillard, A., De Bernardinis, A., Bethoux, O., Hissel, D., Khatir, Z., "A review on DC/DC converter architectures for power fuel cell applications", *Energy Conversion and Management*, 105: 716-730, (2015).
- [10] Kumar, K., Babu, N.R., Prabhu, K.R., "Design and analysis of an integrated Cuk-SEPIC converter with MPPT for standalone wind/PV hybrid system", *International Journal of Renewable Energy Research*, 7(1): 96-106, (2017).
- [11] Saravanan, S., Babu, N.R., "RBFN based MPPT algorithm for PV system with high step up converter", *Energy conversion and Management*, 122: 239-251, (2016).
- [12] Farooq, A., Malik, Z., Qu, D., Sun, Z., Chen, G., "A three-phase interleaved floating output boost converter", *Advances in Materials Science and Engineering*, (2015).  
<http://dx.doi.org/10.1155/2015/409674>
- [13] Ahmed, J., Salam, Z., "An improved perturb and observe (P&O) maximum power point tracking (MPPT) algorithm for higher efficiency", *Applied Energy*, 150: 97-108, (2015).
- [14] Bendib, B., Krim, F., Belmili, H., Almi, M.F., Boulouma, S., "Advanced Fuzzy MPPT Controller for a stand-alone PV system", *Energy Procedia*, 50: 383-392, (2014).
- [15] Ali, U.S., "Z-source DC-DC Converter with Fuzzy Logic MPPT Control for Photovoltaic Applications", *Energy Procedia*, 90: 163-170, (2016).

- [16] Rai, A.K., Kaushika, N.D., Singh, B., Agarwal, N., “Simulation model of ANN based maximum power point tracking controller for solar PV system”, *Solar Energy Materials and Solar Cells*, 95(2): 773-778, (2011).
  
- [17] Kumar, K., Babu, N.R., Prabhu, K.R., “Design and Analysis of RBFN-Based Single MPPT Controller for Hybrid Solar and Wind Energy System”, *IEEE Access*, 5: 15308-15317, (2017).